



Kinetic study of Ni-M/CNT catalyst in methane decomposition under microwave irradiation

Changle Jiang^a, Alazar Araia^a, Sonit Balyan^a, Brandon Robinson^a, Siobhan Brown^a, Ashley Caiola^a, Jianli Hu^{a,*}, Jian Dou^b, Luke M. Neal^b, Fanxing Li^b

^a Department of Chemical and Biomedical Engineering, West Virginia University, Morgantown, WV, United States

^b Department of Chemical and Biomolecular Engineering, North Carolina State University, Raleigh, NC, United States



ARTICLE INFO

Keywords:

Microwave catalysis
Methane decomposition
Carbon nanotubes
Clean hydrogen

ABSTRACT

Methane catalytic decomposition has been studied with catalysts that can attenuate the energy of electromagnetic waves to heat and drive the reaction. Herein, we report, for the first time, a comprehensive kinetic study of Ni-M (M=Pd, Cu, or Fe)-CNT catalysts under microwave irradiation. These binary metal alloy nanoparticles have been synthesized on multiwalled carbon nanotube support with solvothermal process. These catalysts showed incredible performance for both absorbing microwave energy and catalyzing the reaction to form carbon nanotubes and hydrogen. Ni-M-CNT has a reaction order of 0.74. 10Ni-1 Pd-CNT, 10Ni-1Cu-CNT, and 10Ni-1Fe-CNT have activation energies at 87, 75, and 69 kJ/mol. The investigation was carried out in a differential reactor. The results indicated that 10Ni-1Fe-CNT had the lowest activation energy due to the increase in microwave susceptibility. This work pioneered the microwave catalytic methane decomposition field as well as paving the way for future electrification of CO_x-free hydrogen production.

1. Introduction

As the current hydrogen production at the industrial side is dominated by the steam methane reforming, the CO₂ emission generated from this process has become a concern [1–3]. To reduce the carbon emission, the future production of hydrogen could consider methane pyrolysis, which does not release CO₂ and could generate value-added solid carbon that can be sold to compensate the overall hydrogen cost. However, this process is facing carbon deposition issue (carbon fouling) on equipment. With proper catalyst regeneration process, the process has close to zero carbon emission and an easier gas stream separation process, although the coking of the catalyst is also a concern.

Many catalysts have been studied for kinetics of methane catalytic decomposition [4]. The study of activated carbon as a catalyst was carried out in a fixed bed reactor. The study found that the activated carbon has been measured with a reaction order of 0.5 and an activation energy of 117–185 kJ/mol [5]. This was in consistency with the reaction order detected by another work using activated carbon as catalyst for methane decomposition [6], in which the activation energy was measured higher to be 200 kJ/mol. Typically, for methane decomposition, non-catalytic reactions have an activation energy of 356–402

kJ/mol, while the catalytic reactions have an activation energy of 90–236 kJ/mol.

Nickel based catalytic system has been widely used to activate methane molecules. Previously, many catalysts with supported Ni have been used for kinetic study. Ni/SiO₂ with 13 wt% loading Ni had an activation energy of 60 kJ/mol for catalytic methane decomposition [7]. The study also detected that the reaction was first order. 10 wt% Ni supported by Al₂O₃ was used for catalytic methane decomposition between 600 and 750 °C [8]. The reference has adopted temperature-programmed reaction and showed that CNT growth has a peak rate at 690 °C. The work also found in kinetic study that the dissolution of carbon atoms from cracked methane into nickel metal is the rate-limiting step at higher temperatures while the chemisorption of methane onto the metal surface is the limiting step at the lower temperatures. The dissolution-precipitation mechanism of carbon growth has been stressed in this work. A higher loading of 30 % Ni/Al₂O₃ was reported.

Nickel alloy catalyst is a better form of Ni-based catalyst that can significantly improve the catalyst stability and the duration of activity. High loading of Ni-Cu and Ni-Cu-Fe supported by Al₂O₃ has been studied for the methane decomposition. It was found that at 700 °C, 75 %Ni-10

* Corresponding author.

E-mail address: john.hu@mail.wvu.edu (J. Hu).

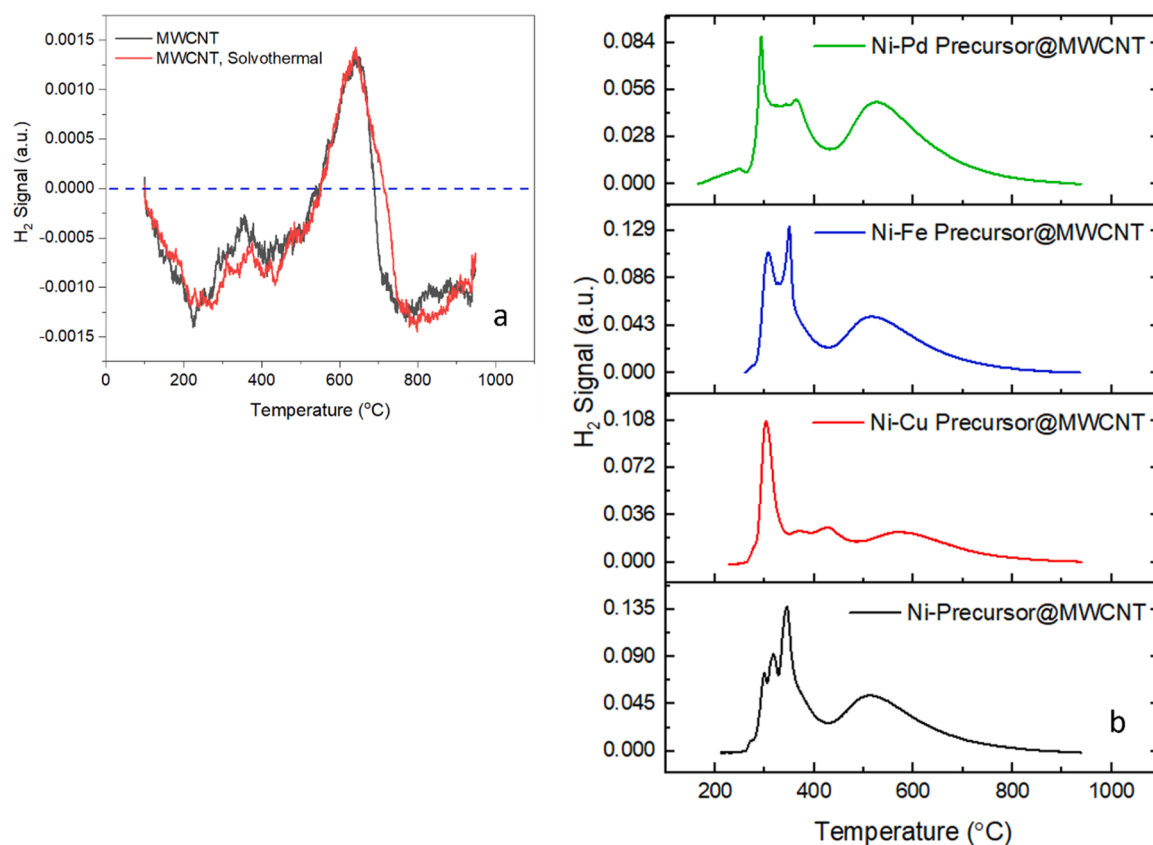


Fig. 1. Temperature programmed reduction in H₂ of catalyst support (a) and catalyst precursors on support (b).

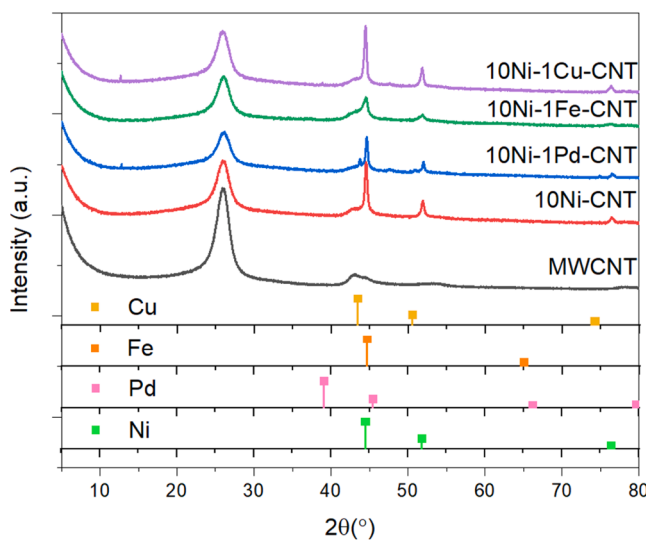


Fig. 2. X-ray diffraction of CNT and catalysts reduced in pure hydrogen flow of 20 ml/min for 4 h.

%Cu-10 %Fe/Al₂O₃ has a duration of activity of 4 h and 3-fold weight gain due to the growth of carbon nanofiber, while compared with the 75 %Ni-12 %Cu/Al₂O₃ [9]. The reported work described that Fe has reduced the initial formation rate of carbon growth while giving the catalyst more stability. In addition, it was found that Fe increased the reaction temperature from 600° to 650°C to 700–750 °C.

Kinetic studies have been carried out to investigate the performance of different Ni based catalysts for the methane catalytic decomposition reactions. In a fixed-bed reactor, Ni and Ni alloy catalysts were

investigated using empirical and exponential decay models and found that the reaction order of Ni was 0.63–0.75, and activation energies were in the range of 64–70 kJ/mol [10]. Ni plating on SBA-15 was studied for kinetics in catalytic methane decomposition, showing an activation energy of 114 kJ/mol and a reaction order of 2 [11]. In the case of fluidization reactor, a commercial Ni catalyst (Ni 5256 E RS, BASF) was measured with an activation energy of 88 kJ/mol with reaction temperature from 550° to 600°C [12].

The idea was to use electromagnetic waves to transfer energy and drive the catalytic reactions. Typically, the catalyst was used as a medium to attenuate the energy from the waves. The process was instant, portable, less energy intensive, and selective heating. Activated carbon was adopted as a feasible medium to absorb microwave for catalyzing the methane decomposition [13–17]. Carbon felt was reported to absorb microwave and generate Y-junction carbon nanotubes at 1100 °C [18]. An Fe-containing carbon absorbent was adopted to convert methane to hydrogen using microwave irradiation at 600 °C and achieved an 84% conversion of methane [19]. The study also proposed that the cleavage of the C-H bond took place on the catalytic surface with the help of the polarization and trans-polarization of the carbon support [20,21]. Our previous work has adopted Ni-CNT catalyst system for microwave catalytic methane decomposition reaction to produce hydrogen and carbon nanotube [22,23]. The results showed that Pd and Cu could significantly improve the conversion of methane and the duration of the catalyst activities.

In this work, Ni-M/CNT catalysts with Ni-M alloy nanoparticles with 10 wt% loading of Ni and 1 wt% of M (M=Pd, Cu, or Fe) loaded on MWCNT support were reported for the first time being evaluated under microwave irradiation for catalytic methane decomposition reactions. The kinetic study on reaction order and activation energy were investigated comprehensively for the first time with the microwave-driven reaction. The improvement of catalyst activity and duration by the

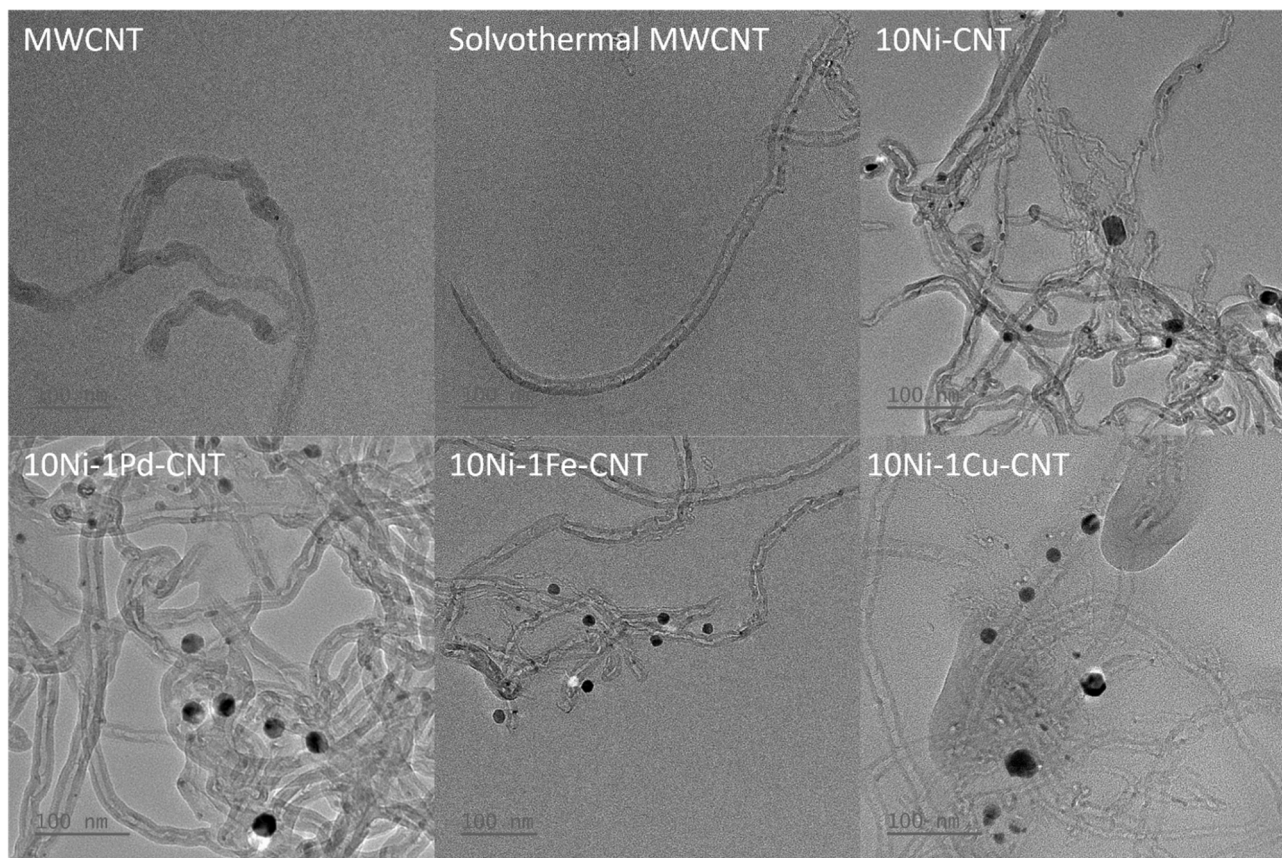


Fig. 3. TEM images of catalyst support and fresh catalysts.

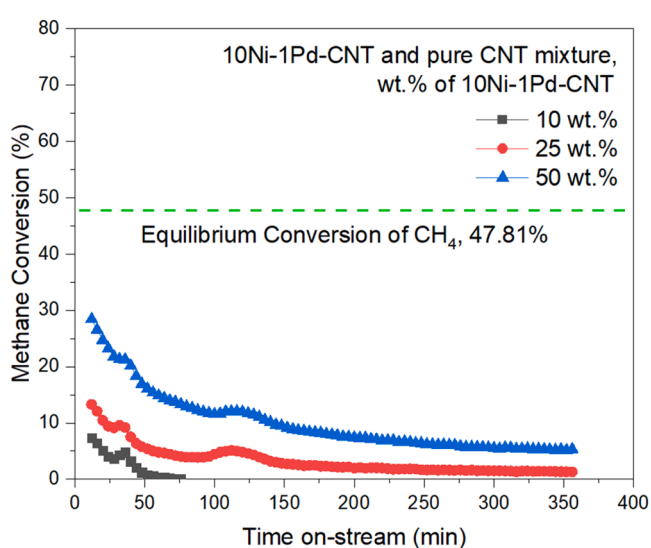


Fig. 4. Methane conversion of microwave catalytic decomposition using diluted 10Ni-1 Pd-CNT catalyst at 500 °C.

promotion effect of M were first reported. The reaction mechanism specifically focused on the interaction of Ni-M/CNT and electromagnetic wave was proposed for the first time in this work.

2. Experimental section

2.1. Materials

Multiwalled carbon nanotubes (MWCNT) were purchased from Cheap Tubes Inc (Grafton, Vermont, USA). The work will refer to the MWCNT as CNT herein. The CNTs have an outer diameter of 20–30 nm, and an inside diameter of 5–10 nm. The length is 10–30 μm. It has an ash content of 1.5 wt% or less. Purity is larger than 95 wt%. The specific surface area is 110 m²/g. Electrical conductivity is 100 S/cm or larger. It has a bulk density of 0.28 g/cm³. The true density is about 2.1 g/cm³. Catalyst precursor Ni(NO₃)₂·6 H₂O, Pd(NO₃)₂·2 H₂O, Fe(NO₃)₃·9 H₂O, and Cu(NO₃)₂·2.5 H₂O were purchased from Sigma Aldrich.

2.2. Catalyst preparation

CNT supported Ni-M catalysts were prepared using a solvothermal process with acetone as solvent. Catalyst precursor Ni(NO₃)₂·6 H₂O, Pd(NO₃)₂·2 H₂O, Fe(NO₃)₃·9 H₂O, and Cu(NO₃)₂·2.5 H₂O were dissolved into 50 ml acetone, stirred and sonicated for 20 min separately. Then, CNTs were added into the solution, stirred and sonicated for 20 min separately. The as-prepared suspension was placed into a 100 ml Teflon and moved into a sealed autoclave. The autoclave was heated in an oven to 120 °C and held at the temperature for 12 h. The resultant suspension was air-dried for 12 h, then oven-dried for 12 h after the suspension became slurry. Eventually, the dried CNT supported precursors underwent reduction at 400 °C for 4 h in pure hydrogen flow with a rate of 20 ml/min in a tube furnace. The as-prepared catalyst from the reduction will be referred to fresh catalyst. The fresh catalyst will be used in the methane decomposition reaction. The catalyst after the reaction will be referred to as the spent catalyst.

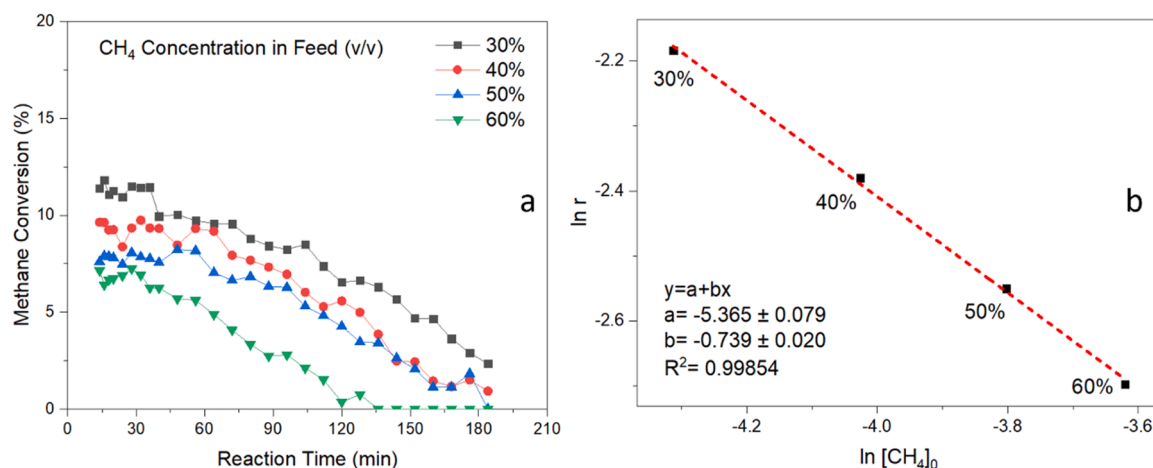


Fig. 5. (a) Methane conversion with 10Ni-1 Pd-CNT under conventional heating at 475 °C, (b) correlation of $\ln r$ and $\ln [\text{CH}_4]_0$ of 10Ni-1 Pd-CNT.

Table 1

Measured reaction rates at 20 min under different initial CH₄ concentrations ($T = 475^\circ\text{C}$).

Inlet CH ₄ Conc. (v/v)	r at 20 min TOS	$\ln r$	[CH ₄] ₀ (mol/L/min)	$\ln [\text{CH}_4]_0$
30 %	0.11261	-2.184	1.339E-2	-4.313
40 %	0.09259	-2.380	1.785E-2	-4.026
50 %	0.07808	-2.550	2.232E-2	-3.802
60 %	0.06741	-2.697	2.678E-2	-3.620

2.3. Microwave catalytic methane decomposition

The methane decomposition in this work was driven by the heat generated from the interaction between the catalyst and electromagnetic wave. In this work, the frequency of the microwave generator was 5.85 GHz for all the tests. The catalyst was placed in a fixed-bed reactor, which was inserted into a microwave waveguide (Lambda Technologies). The catalyst bed was aligned with the waveguide, then the microwave heating began. The heating process was programmed with default software. The temperature was measured at two locations of the reactor: one is the temperature of the catalyst bed inside the reactor. The other is the temperature of the reactor wall. Both were detected with a pyrometer and controlled by computer software. The scheme of experimental equipment has been added to the [supplementary materials](#) file (Fig. S1). The ramping rate was 0.2 °C/s. The reaction temperature for

the methane decomposition was within a range of 400–500 °C for the data collection of methane conversion. The gas feed consisted of methane and nitrogen. The conversion data under different methane concentrations were collected for the calculation of reaction order. The conversion data under different reaction temperatures were collected for the calculation of the activation energy. The conversion data were

Table 2

Data used for modeling of activation energy of 10Ni-1 Pd-CNT.

Reaction Temperature (°C)	1/T (1/K)	$\ln k$
475	0.00134	4.53726
450	0.00138	4.04429
425	0.00143	3.67361
400	0.00149	2.92782

Table 3

Data used for modeling of activation energy of 10Ni-1Cu-CNT and 10Ni-1Fe-CNT.

Catalyst	Reaction temperature (°C)	1/T (1/K)	$\ln k$
10Ni-1Cu-CNT	500	0.00138	3.51128
	475	0.00134	3.91757
	450	0.00129	4.3199
10Ni-1Fe-CNT	500	0.00129	5.17087
	450	0.00138	4.52703
	400	0.00149	3.58701

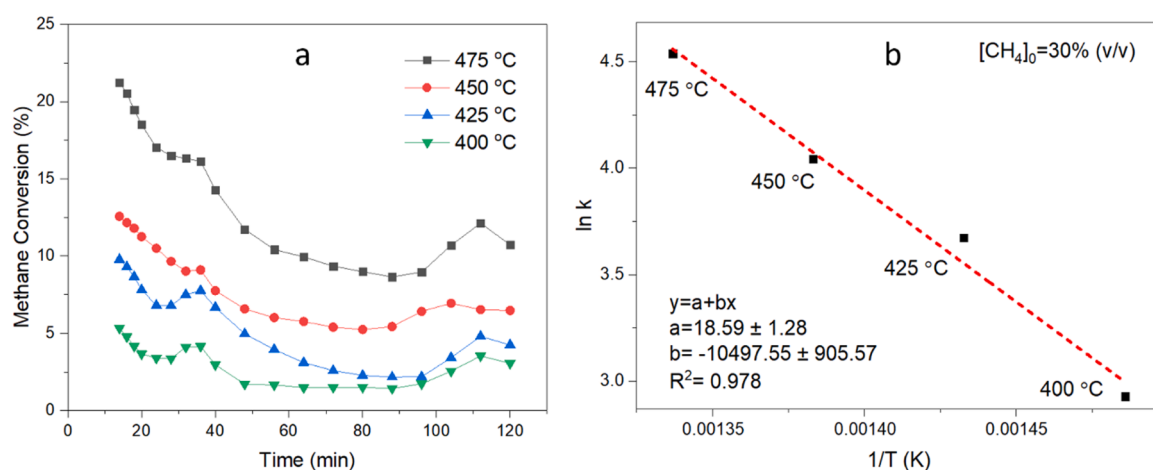


Fig. 6. (a) Methane conversion data of 10Ni-1 Pd-CNT in a differential reactor; (b) correlation of $\ln k$ and $1/T$ for 10Ni-1 Pd-CNT.

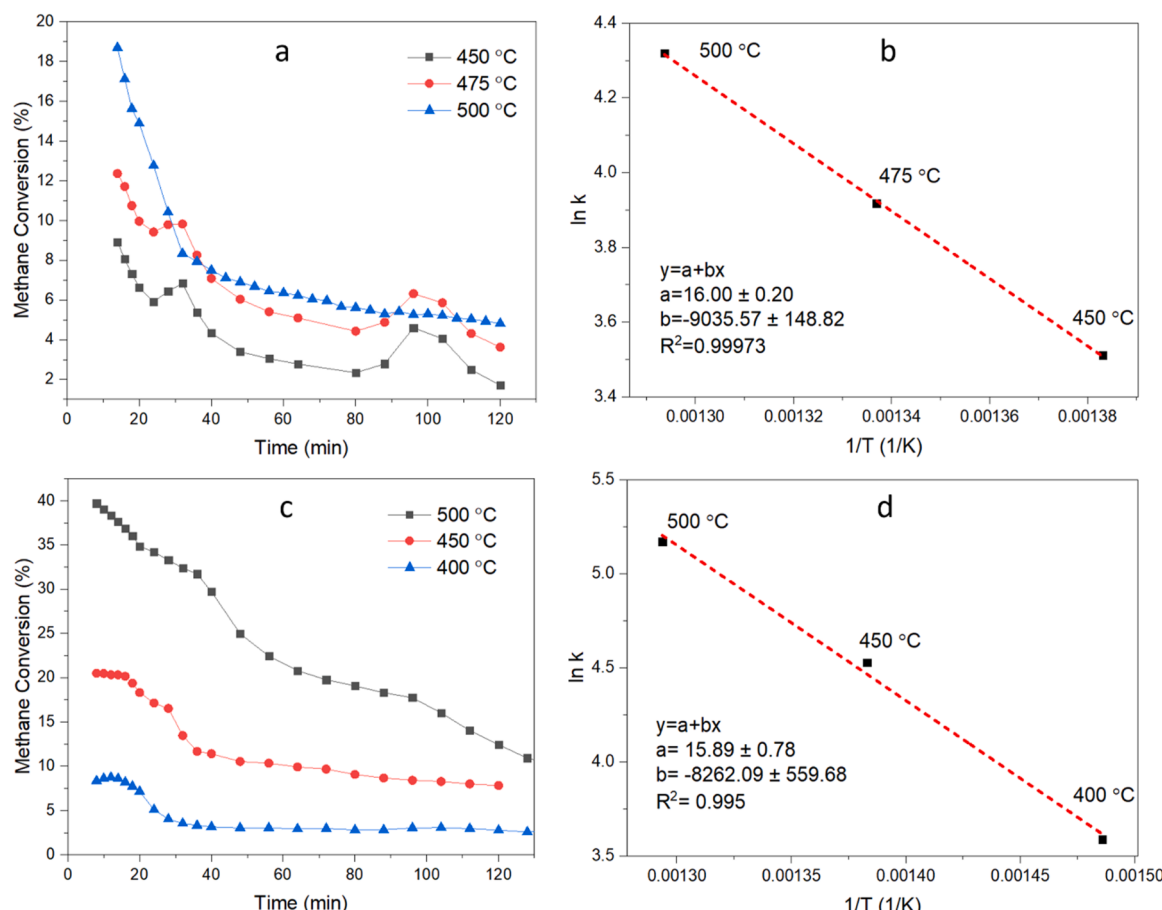


Fig. 7. (a) Methane conversion data of 10Ni-1Cu-CNT; (b) correlation between $\ln k$ and $1/T$ of 10Ni-1Cu-CNT; (c) methane conversion data of 10Ni-1Fe-CNT; (d) correlation between $\ln k$ and $1/T$ of 10Ni-1Fe-CNT.

collected in a fixed-bed setup of a differential reactor. The active catalyst 10Ni-1 M-CNT was 0.05 g. The CNTs used as dilutant and microwave absorbing enhancer of 0.15 g was added. The reason for adding extra CNTs was that 0.05 g of active catalyst was not able to fill the waveguide width. An extra 0.15 g of CNTs was added. This portion of solid materials were only for heating purposes. The CNTs themselves are quite inert for the methane decomposition reaction. Methane conversion was calculated using the same method as described in our previous work using nitrogen as an internal standard [22].

2.4. Transmission electron microscopy (TEM)

The fresh catalyst of 10Ni-CNT, 10Ni-1 Pd-CNT, 10Ni-1Cu-CNT, 10Ni-1Fe-CNT have been observed with TEM for morphology. In addition, the CNTs before and after solvothermal treatment with acetone in 120 °C autoclave for 12 h was imaged. Note that all CNT support in this work was multiwalled carbon nanotubes. The catalyst samples were dispersed in acetone solutions to form suspension, which was later dropped onto the TEM grid for imaging. The TEM used in this work was JEOL JEM-2100 that operated with an accelerating voltage of 200 kV. The metal particle size has been measured using TEM images at 50 nm scale over minimum 6 particles on each image of the samples.

2.5. Temperature programmed reduction

Temperature programmed reduction of catalyst precursors supported by CNTs were conducted with Micromeritics Autochem HP 2950. Hydrogen was flowed as the reduction agent. 0.05 g of CNT supported catalyst precursors were purged with 30 ml/min nitrogen at 150 °C for

60 min. Upon purging, the catalyst samples were ramped to 900 °C at a rate of 10 °C/min under 30 ml/min 10 % hydrogen in argon flow.

2.6. X-ray diffraction analysis (XRD)

The XRD analysis was carried out to investigate the crystal structure of the Ni-M on the MWCNT. The crystal structure has a great influence on the chemisorption of methane molecules onto the surface of Ni-M and determines the rate of dissolution of carbon onto metal surface. The analysis was conducted on PANalytical X'Pert Pro X-ray Diffractometer. The equipment has Cu- κ source and Maximum X-Ray power of 45 kV and 40 mA. It has an angular range of $5^\circ < 2\theta < 110^\circ$. It has Highscore Plus analysis software with PDF 3 database. A spinning sample stage was used.

2.7. Surface area

The surface areas of the catalysts were characterized using Micromeritics ASAP 2020 + (Micromeritics Instrument Corp). The surface areas of the pure CNT, 10Ni-1 Pd-CNT, 10Ni-1Cu-CNT, 10Ni-1Fe-CNT were calculated with the Brunauer-Emmett-Teller (BET) model. These samples were degassed at 300 °C for 6 h. Nitrogen adsorption and desorption test was carried out using the same equipment to measure the surface area of the samples.

2.8. Kinetic study of methane decomposition

The kinetic study was referred to our previous work (Jiang et al., 2012). The reaction order was calculated by the slope resulted from the

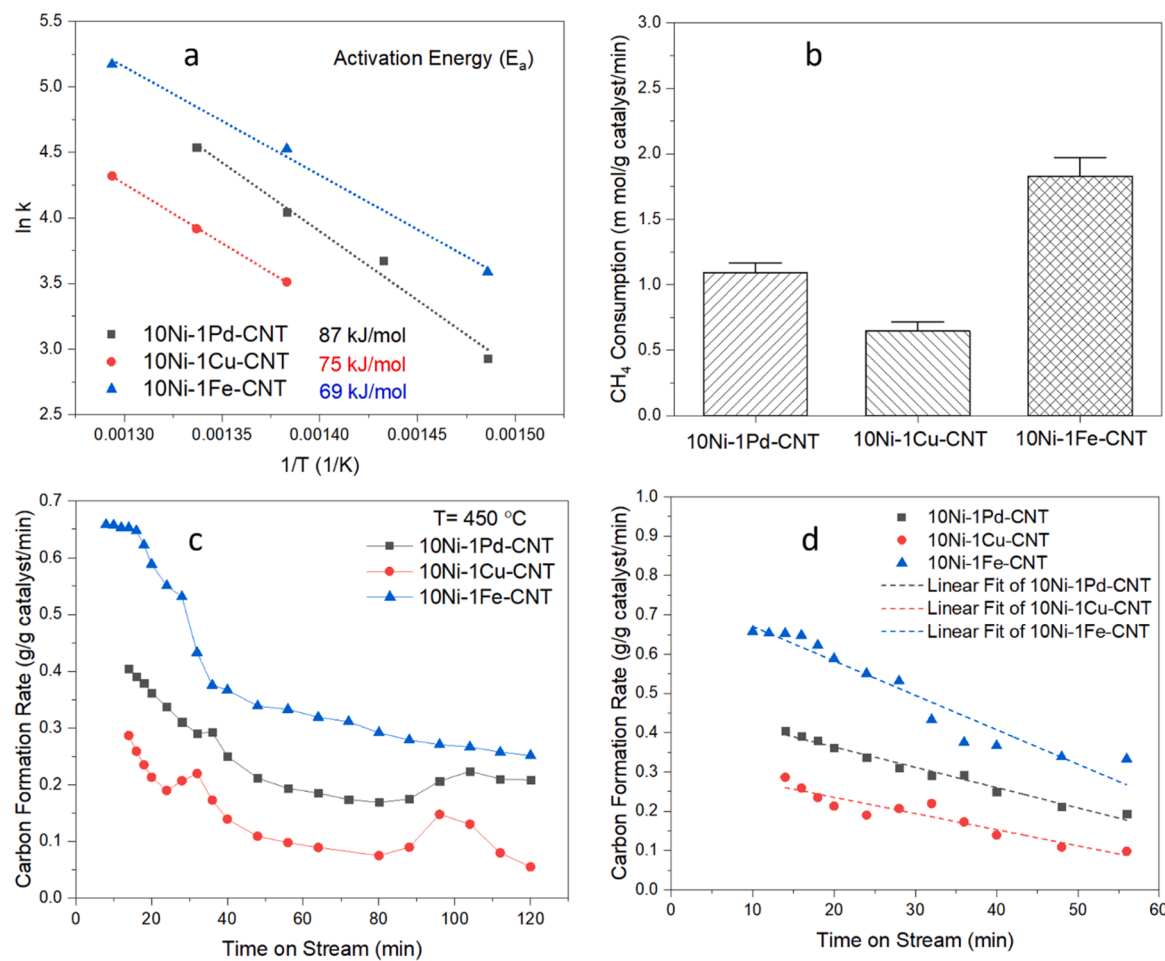


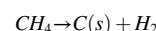
Fig. 8. Comparison of Ni-M-CNT performance under microwave irradiation: (a) activation energies of three catalysts tested, (b) efficiencies of three catalysts, (c) carbon formation rate of catalysts, and (d) deactivation of catalysts.

Table 4

The linear model for catalyst deactivation of Ni-M-CNT under microwave in initial 1 h of TOS shown in Fig. 8d.

Equation	$y = a + bx$	10Ni-1 Pd-CNT	10Ni-1Cu-CNT	10Ni-1Fe-CNT
Catalyst	10Ni-1 Pd-CNT	$10Ni-1Cu-CNT$	$10Ni-1Fe-CNT$	
Intercept	0.467 ± 0.008	0.318 ± 0.016	0.751 ± 0.020	
Slope	$-0.0052 \pm 2.5E-4$	$-0.0041 \pm 4.7E-4$	$-0.0086 \pm 6.7E-4$	
R ²	0.97799	0.88253	0.92583	

plotting reaction rate of methane ($\ln r$) against different methane partial pressure ($\ln [CH_4]_0$). Thus, the reaction order n can be determined as the slope of linear fitting between $\ln r$ and $\ln [CH_4]_0$. The calculation was carried out using Eqs. (1 and 2). The reaction order has been carried out in a differential reactor with only 0.05 g of Ni/CNT catalyst. It was also assumed that the reaction order was mainly determined by 10 %Ni, rather than 1 wt% M. However, the activation energy could be significantly influenced by the 1 wt% M. The activation energies of Ni-M/CNT catalysts were calculated with conversion data from microwave-driven catalytic methane decomposition reactions under different reaction temperature from 400° to 500°C. The calculation of activation energy was based on the Arrhenius equation. The rearrangement of the reaction was used to plot linear regression between $\ln k$ and $1/T$. The slope of the plotting was $-E_a/R$. R was the universal gas constant. Thus, E_a can be further calculated. The measurement of E_a was carried out with Eqs. (3–6).



For reaction order, rate law was adopted:

$$r = k \times [CH_4]_0^n \quad (1)$$

Linear regression between $\ln r$ and $\ln [CH_4]_0$ was used for the plotting:

$$\ln r = n \times \ln [CH_4]_0 + \ln k \quad (2)$$

Where,

r is the reaction rate of CH_4 .

$[CH_4]_0$ is the initial partial pressure of CH_4 .

k is rate constant.

n is reaction order.

For activation energy, Arrhenius equation was applied:

$$k = Ae^{\frac{-E_a}{RT}} \quad (3)$$

It can be rearranged to:

$$\ln k = -\frac{E_a}{R} \left(\frac{1}{T} \right) + \ln A \quad (4)$$

$$b = -\frac{E_a}{R} \quad (5)$$

Activation energy can be calculated as:

$$E_a = -R * b \quad (6)$$

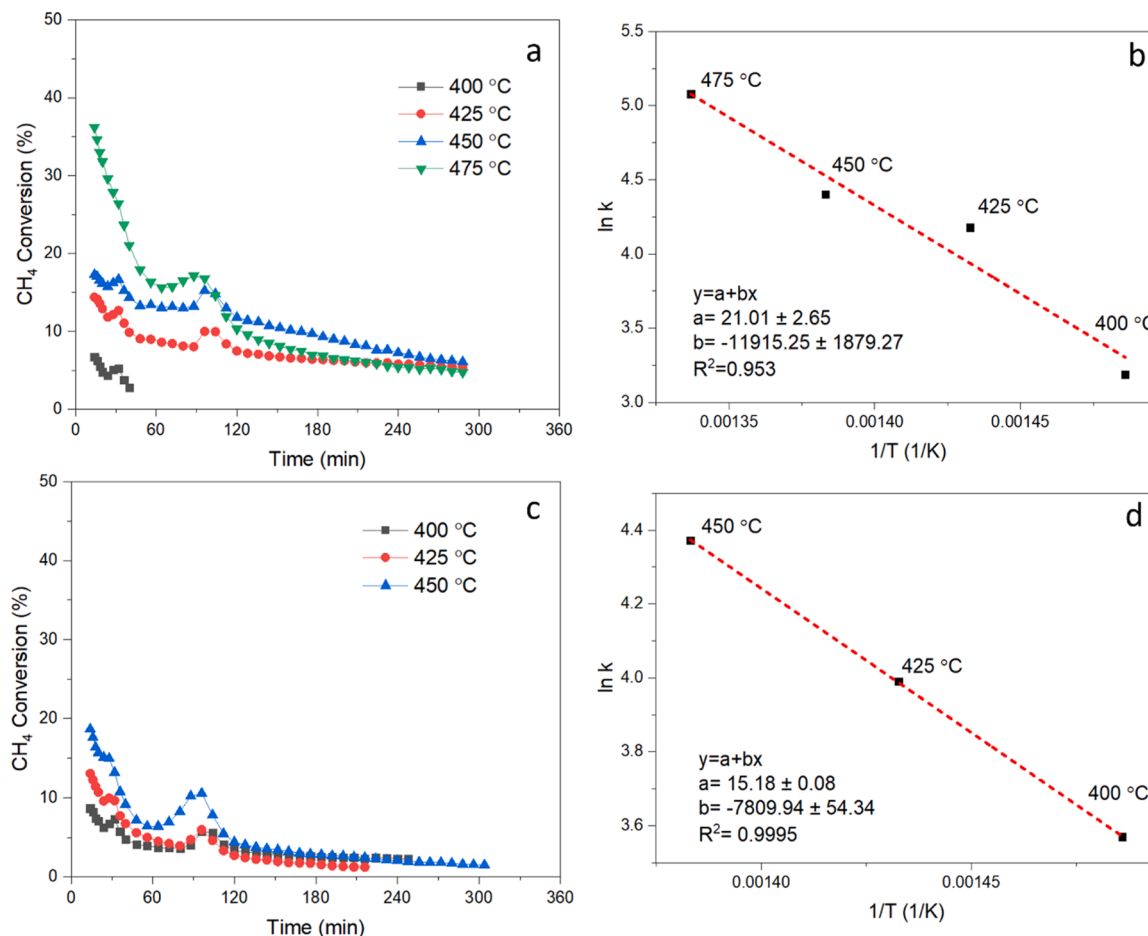


Fig. 9. The effect of solvothermal temperatures on the E_a of 10Ni-CNT catalyst: (a) methane conversion of 10Ni-CNT catalyst prepared at 90 °C, (b) activation energy fitting of 10Ni-CNT catalyst prepared at 90 °C, (c) methane conversion of 10Ni-CNT catalyst prepared at 120 °C, and (d) activation energy fitting of 10Ni-CNT catalyst prepared at 120 °C.

Where,

- k is reaction rate constant, depending only on reaction temperatures.
- E_a is the activation energy.
- $1/T$ is the reciprocal of reaction temperatures.
- A is the pre-exponential factor.
- R is the universal gas constant.
- T is the absolute reaction temperature (in Kelvin).
- b is the slope of linear fitting between $\ln k$ and $1/T$ equals $-E_a/R$.

3. Results and discussion

3.1. Characterizations of the prepared catalysts

The precursor of Ni and Ni-M (Cu, Fe, Pd) were loaded on the MWCNT after the solvothermal process in autoclave using acetone as the solvent. As the solvent evaporated, the solid catalyst precursors loaded on MWCNT were oven dried. The reduction of the catalyst precursors was conducted in a fixed-bed tube furnace in pure hydrogen flow with H₂ flow of 20 ml/min for 4 h. The reduction process has been simulated with a temperature programmed reduction (TPR) process with H₂ flow. The equipment measured the signal of H₂ with a thermal conductivity detector (TCD). The related data for this TCD can be referred to Table S1 and Fig. S2 in the Supplementary Material file. The H₂ signal against the reduction temperature profile was displayed in Fig. 1. First, MWCNT samples before and after solvothermal process were tested with the TPR process to find out if there was any H₂ intake during the reduction of the MWCNT samples. Fig. 1a data indicated that there is no intake of

hydrogen since the fluctuation of the consumption signal was within ± 0.0015 , which was within the error margin. Note that this result has ruled out the interference of MWCNT on the consumption of the H₂ later measured with catalyst precursors. Fig. 1b showed the H₂ consumption signal of all precursors. Nitrate groups decomposed from 75° to 265°C [24]. However, this process did not consume H₂, thus, no signal of H₂ consumption was shown. The nickel nitrate became NiO after 300 °C. PdO_x and CuO_y were both reduced to Pd and Cu before 300 °C, respectively [25,26]. FeO_z reduction in H₂ spans longer on temperature than PdO_x and CuO_y. However, 1 wt% of these metal oxides would have few influences on the peaks of reduction. The peaks in Fig. 1b were primarily due to the reduction of NiO. All these peaks can generally be separated into two NiO groups: 300–500 °C for the reduction of α -NiO and 500–600 °C for the reduction of β -NiO [27]. Both types had a weak interaction with the CNT.

The XRD analysis in Fig. 2 has showed that all the fresh catalysts showed the characteristic peaks of Ni nanoparticles at 44.5, 51.8 and 76.4 degrees of 2θ, which is in consistency with the results reported for the analysis of these nanoparticles [28–30], indicating the nickel nanoparticles were successfully synthesized on the MWCNT support. It is worth noting that the second metal (M) only had a weight percentage of 1 wt%, thus, was not visible on XRD spectra. Particle size, surface area, and metal loading of the catalysts can be found on Table S2 in Supplementary Material file.

Morphology of the catalyst support and fresh catalysts has been characterized by the transmission electron microscope (TEM), as shown in Fig. 3. MWCNT as purchased has < 1.5 % ash content, which did not

post any influence on the conversion of the methane. MWCNT has been tested to catalyze the methane decomposition reaction under microwave, resulting in a negligible methane conversion (<1%). The MWCNT has an outer diameter of 20–30 nm and an inside diameter of 5–10 nm. The length of the tube is 10–30 μm . The specific surface area is 110 m^2/g . The electrical conductivity is > 100 S/cm. The morphology of catalyst support MWCNT was examined before and after the solvothermal process using acetone as a solvent. The catalyst has been pressurized with acetone liquid and vapor inside the autoclave, which was reported to synthesize more desired size of nanoparticles of Ni over other solvents like water, ethanol, and butanol [31]. The mechanism was proposed in this reference that the chelation between acetone and Ni ion facilitated the growth of NiO, which can later be reduced to Ni nanoparticles upon reduction in pure hydrogen flow. Upon comparison of the physical appearances of MWCNT before and after the solvothermal treatment, it has indicated that the physical structure of MWCNT was not affected by the process. MWCNT can hold the pressure and temperature within the autoclave, showing great stability for being a catalyst support material. The reduction of the Ni precursors supported by MWCNT was carried out in a 20 ml/min pure hydrogen flow. The distribution of the Ni nanoparticles after the reduction on the MWCNT has been displayed in Fig. 3. The size of the Ni ranged from 10 to 30 nm. Upon adding 1 wt% M (M=Pd, Fe, or Cu), the resulting Ni-M alloy metal particles have a size range of 10–30 nm as well. The 10Ni-1Fe-CNT showed slightly smaller size of nanoparticles within the range.

3.2. Differential reactor test of 10Ni-1 Pd-CNT

10Ni-1 Pd-CNT has a methane conversion of > 30 % at 550 °C [22], which is not suitable for the kinetic study for reaction order and activation energy. To qualify for the differential reactor scenario, the mass of 10Ni-1 Pd-CNT must be as small as possible. Although in some experimental runs it was not ideal, the methane conversion must be controlled to a relatively low level as possible. Therefore, a solid dilution method was adopted to study the kinetics of 10Ni-1 Pd-CNT. The method used MWCNT, which was the catalyst support during the preparation, to act as a dilution solid. MWCNT is inert toward the methane decomposition reaction. The microwave zone has a width of ~1 cm. Before adding MWCNT, the 0.05 g active 10Ni-1 Pd-CNT could not fill up the microwave zone. Upon adding MWCNT, the total width of the catalyst bed could reach 1 cm, which covered the width of the microwave zone. The methane conversion results of tests with diluted catalysts that contained 10 wt%, 25 wt%, and 50 wt% of 10Ni-1 Pd-CNT was displayed in Fig. 4a. The 10 wt% 10Ni-1 Pd-CNT has experienced a fast deactivation, which has been disqualified for the kinetic study. The 50 wt% dilution has a relatively high methane conversion, which was not selected. Upon the screening tests, the 25 wt% 10Ni-1 Pd-CNT was optimized as the suitable solid dilution ratio for further kinetic study. The CNT support has been used as control catalyst for both conventional and microwave heating. The results have been shown in Fig. S3 in [Supplementary Material file](#). We did not detect any acetylene in any methane decomposition runs in our work. Typically, without oxidant, methane coupling to acetylene would require a much higher temperature than the reaction temperatures in our current study.

3.3. Measurement of reaction order for 10Ni-1 Pd-CNT

The measurement of reaction order was carried out with 25 wt% 10Ni-1 Pd-CNT in a differential reactor under conventional heating. The methane conversion data was shown in Fig. 5a. As the initial methane concentration increased, the methane conversion decreased. The conversion data collected at 20 min was adopted for the reaction rate (r). The data used for the correlation, as shown in Fig. 5b, between the $\ln r$ and $\ln [\text{CH}_4]_0$ was listed in Table 1. The reaction order (n) was measured as 0.74. n is independent of reaction temperature. It is also independent of the way of heating [22]. The reaction order is independent of reaction

temperature. We have used the rate law to determine the reaction order, as shown in Eqs. (1 and 2). Typically, the rate constant k will be dependent on reaction temperature. Microwave heating or conventional heating will not affect the k at a given reaction temperature. Thus, when we measured our reaction order at a certain reaction temperature with either microwave heating or conventional heating, k is constant, and so is $\ln k$. Thus, n remains the same in both thermal and microwave heating. It is adopted for further activation energy determination in both thermal and microwave heating scenarios. The same reaction order was measured in a previous study that has studied the initial rate of methane decomposition, and showed that it was proportional to the methane pressure with an order of 0.74 ± 0.19 for Ni nanoparticle [32]. 1 wt% Cu and Fe in 10Ni-1Cu-CNT and 10Ni-1Fe-CNT did not change the crystal structure of the Ni nanoparticles as shown in the XRD spectra. Thus, the reaction order should be extremely close to 0.74.

3.4. Activation energy of 10Ni-1 M-CNT

The methane conversion data of this dilution ratio were further collected with reaction temperature ranging from 400° to 475°C, shown in Fig. 6a. This data has been used for the modelling of activation energy for 10Ni-1 Pd-CNT under microwave irradiation using a linear regression, shown in Fig. 6b. Slope b of this fitting was solved as 10, 497 \pm 905, with an R-square of 0.978. Based on Eq. (5), Eq. (6), and universal gas constant R (8.3145 J/mol/K), E_a was calculated as 87.3 kJ/mol. The measurement of activation energy was carried out with initial methane partial pressure at 0.3 (30 % v/v in a CH₄/N₂ feed). Nitrogen was only used for internal standard purposes in the MicwoGC analysis. (Table 2).

The measurement of the activation energy was carried out with an optimized catalyst layout inside the same differential reactor. The reaction order remained at 0.74 since change of catalyst composition would not change the reaction order. The reaction order was also largely determined by the similar Ni ratios in these three binary metallic catalysts. After all, the reaction order was dominated by the rate-limiting/determining step: the dissolution of carbon from methane molecular and into the surface of the 10 wt% Ni, where the 1 wt% promoter would not have much influence on. However, the activation energy could be affected by this 1 wt% promoter since the promotor could reduce the energy barrier for the rate-limiting step, making it take place at a lower reaction temperature requirement. (Table 3).

The 0.05 g of each 10Ni-1Cu-CNT and 10Ni-1Fe-CNT catalyst were placed between two 0.075 g (total 0.150 g) MWCNT layers during the loading of the catalyst into the reactor, forming a sandwich structure. The 10Ni-1Cu combination has a calculated E_a of 75.1 kJ/ml, with a reaction temperature of 450–500 °C. The 10Ni-1Fe combination has a calculated E_a of 68.7 kJ/mol, with a reaction temperature of 400–500 °C. From the methane conversion data shown in Figs. 7a and 7c, it clearly indicates that the 10Ni-1Fe combination has higher activity. In addition, the 10Ni-1Fe-CNT catalyst has shown that it can work under lower reaction temperatures. As indicated by the activation energy comparison between different promoters of Pd, Cu, and Fe, the 10Ni-1Fe-CNT displayed the lowest activation energy.

Unsupported Ni and Ni-Co-Cu alloy catalyst were studied with respect to the deactivation process [10]. The report has measured the reaction order of unsupported Ni particles at 450 °C with methane initial partial pressure from 0.2 to 0.8. The results showed that the reaction order of Ni catalyst has an average reaction order of 0.63. The reaction order of unsupported 2Ni-1Co-1Cu was measured as 0.75. The activation energy of Ni, and 2Ni-1Co-1Cu was reported in this reference as 65.4 and 67.5 kJ/mol, respectively. Ni_xCu_y-CNT catalyst was synthesized with a polyol reduction method from the same research group had a best working temperature from 727° to 752°C, depending on the x/y ratios [33]. The average activation energy of these Ni-Cu-CNT catalyst was 99 kJ/mol. This reference also reported that an activation energy of 52 kJ/mol was measured for Ni-CNT prepared in the work.

The performance evaluation of the catalysts developed in this work was shown in Fig. 8. A direct comparison of three promoters indicated that the 1 wt% Fe could achieve the lowest activation energy (shown in Fig. 8a). The methane consumption rate in Fig. 8b further showed that Ni-Fe combination could consume about 1.8 m mol of methane per min, which was visibly higher than Ni-Pd or Ni-Cu combinations. The carbon formation rate at reaction temperature 450 °C was displayed in Fig. 8c. The methane consumption and carbon formation rates were measured based on the data collected in 2 h. The deactivation evaluation was using the data collected in the initial 1 h since the carbon formation rate in the second hour plateaued. The carbon formation rate and time was modeled with linear regression. The results were displayed in Fig. 8d and Table 4. The results indicated that although 10Ni-1Fe-CNT performed better with lower reaction temperature, lower activation energy, higher methane conversion and carbon formation rates, it has experienced more severe deactivation rate in the first hour of reaction. It was reported that Ni-Fe tended to have a higher saturation magnetization than Ni-Cu or Ni-Pd in general, which might help facilitate the carbon dissolution process on the metal surface [34,35]. Similar Ni-Fe coated carbon nanofiber was reported to be used as a loss enhancement layer for microwave absorbing composite materials [36–38].

3.5. Effect of solvothermal temperature on activation energy of 10Ni-CNT

The catalysts from the above content were all prepared with a solvothermal temperature of 120 °C. To have a clear look at the different of E_a due to the catalyst preparation temperature, deactivation of 10Ni-CNT in the absence of promoter was studied with solvothermal process temperatures 90 and 150 °C to have a definitive comparison of the catalysts prepared with two different temperatures (Fig. 9). The 10Ni-CNT catalyst prepared at 90 °C had an E_a of 99.1 kJ/mol while the one prepared at 150 °C had an E_a of 64.9 kJ/mol. Higher temperatures of the solvothermal process were reported to slowly form crystalline NiO, even before the reduction step at higher temperature in hydrogen, on the catalyst support from the chelation complex between Ni ion and organic ligands [31,39].

4. Conclusion

This work has developed three binary Ni based catalysts for methane catalytic decomposition under dielectric heating. The XRD characterization of the prepared catalyst all showed a dominated characteristic Ni peak for the alloy catalyst. The measured reaction order was 0.74 for Ni-M-CNT catalysts, which was consistent with the previous reference working on the similar topic. The activation energy of the different Ni-M-CNT combination was measured, and it has indicated that the 1 wt % Fe (M) could achieve the lowest E_a of 64.9 kJ/mol when compared with same weight percentages of Pd or Cu. In addition, Fe is at a much lower price when compared with Pd or Cu. It was also found that Fe has a lower working temperature requirement compared with Pd or Cu. Ni-Fe-CNT combination has been optimized as the best catalyst for the microwave-driven methane catalytic decomposition.

CRediT authorship contribution statement

Changle Jiang: Conceptualization, Investigation, Methodology, Formal analysis, Data curation, Writing – original draft, Writing – review & editing. **Alazar Araia:** Investigation, Methodology, Formal analysis. **Sonit Balyan:** Investigation, Methodology, Formal analysis. **Brandon Robinson:** Investigation, Methodology, Formal analysis. **Siobhan Brown:** Investigation, Methodology, Formal analysis. **Ashley Caiola:** Investigation, Methodology, Formal analysis. **Jianli Hu:** Writing – review & editing, Supervision, Project administration, Funding acquisition. **Jian Dou:** Investigation, Methodology, Formal analysis. **Luke M. Neal:** Methodology. **Fanxing Li:** Project administration, Funding acquisition.

Declaration of Competing Interest

The authors declare that they have no known competing financial interests or personal relationships that could have appeared to influence the work reported in this paper.

Data availability

No data was used for the research described in the article.

Acknowledgement

The authors acknowledge the financial support from the US Department of Energy under the contract #DE-FE-0031866. The authors also would like to thank Dr. Marcela Redigolo and Dr. Qiang Wang from West Virginia University Shared Research Facility for their help regarding TEM and XRD analysis.

Appendix A. Supporting information

Supplementary data associated with this article can be found in the online version at doi:10.1016/j.apcatb.2023.123255.

References

- [1] B. Chen, Z. Liao, J. Wang, H. Yu, Y. Yang, Exergy analysis and CO₂ emission evaluation for steam methane reforming, Int. J. Hydrog. Energy 37 (2012) 3191–3200, <https://doi.org/10.1016/j.ijhydene.2011.10.102>.
- [2] B. Lumbars, D.W. Agar, J. Gebel, F. Platte, Mathematical modelling and simulation of the thermo-catalytic decomposition of methane for economically improved hydrogen production, Int. J. Hydrog. Energy 47 (2022) 4265–4283, <https://doi.org/10.1016/j.ijhydene.2021.11.057>.
- [3] I. Wang, R.A. Dagle, T.S. Khan, J.A. Lopez-Ruiz, L. Kovarik, Y. Jiang, M. Xu, Y. Wang, C. Jiang, S.D. Davidson, P. Tavadze, L. Li, J. Hu, Catalytic decomposition of methane into hydrogen and high-value carbons: combined experimental and DFT computational study, Catal. Sci. Technol. 11 (2021) 4911–4921, <https://doi.org/10.1039/d1cy00287b>.
- [4] Y. Li, D. Li, G. Wang, Methane decomposition to CO_x-free hydrogen and nano-carbon material on group 8-10 base metal catalysts: a review, Catal. Today 162 (2011) 1–48, <https://doi.org/10.1016/j.cattod.2010.12.042>.
- [5] Z. Bai, H. Chen, B. Li, W. Li, Catalytic decomposition of methane over activated carbon, J. Anal. Appl. Pyrolysis 73 (2005) 335–341, <https://doi.org/10.1016/j.jaatp.2005.03.004>.
- [6] M.H. Kim, E.K. Lee, J.H. Jun, S.J. Kong, G.Y. Han, B.K. Lee, T.J. Lee, K.J. Yoon, Hydrogen production by catalytic decomposition of methane over activated carbons: kinetic study, Int. J. Hydrog. Energy 29 (2004) 187–193, [https://doi.org/10.1016/S0360-3199\(03\)00111-3](https://doi.org/10.1016/S0360-3199(03)00111-3).
- [7] S.H.S. Zein, A.R. Mohamed, P.S.T. Sai, Kinetic studies on catalytic decomposition of methane to hydrogen and carbon over Ni/TiO₂ catalyst, Ind. Eng. Chem. Res. 43 (2004) 4864–4870, <https://doi.org/10.1021/ie034208f>.
- [8] M. Inoue, K. Asai, Y. Nagayasu, K. Takane, S. Iwamoto, E. Yagasaki, K. Ichi Ishii, Formation of multi-walled carbon nanotubes by Ni-catalyzed decomposition of methane at 600–750 °C, Diam. Relat. Mater. 17 (2008) 1471–1475, <https://doi.org/10.1016/j.diamond.2008.01.074>.
- [9] V.V. Chesnokov, A.S. Chichkan, Production of hydrogen by methane catalytic decomposition over Ni-Cu-Fe/Al₂O₃ catalyst, Int. J. Hydrog. Energy 34 (2009) 2979–2985, <https://doi.org/10.1016/j.ijhydene.2009.01.074>.
- [10] H.Y. Wang, A.C. Lua, Deactivation and kinetic studies of unsupported Ni and Ni-Co-Cu alloy catalysts used for hydrogen production by methane decomposition, Chem. Eng. J. 243 (2014) 79–91, <https://doi.org/10.1016/j.cej.2013.12.100>.
- [11] Q. Chen, A.C. Lua, Kinetic reaction and deactivation studies on thermocatalytic decomposition of methane by electroless nickel plating catalyst, Chem. Eng. J. 389 (2020), 124366, <https://doi.org/10.1016/j.cej.2020.124366>.
- [12] M. Hadian, D.P.F. Marreeve, K.A. Buist, B.H. Reesink, A.N.R. Bos, A.P. van Bavel, J. A.M. Kuipers, Kinetic study of thermocatalytic decomposition of methane over nickel supported catalyst in a fluidized bed reactor, Chem. Eng. Sci. 260 (2022), 117938, <https://doi.org/10.1016/j.ces.2022.117938>.
- [13] A. Domínguez, B. Fidalgo, Y. Fernández, J.J. Pis, J.A. Menéndez, Microwave-assisted catalytic decomposition of methane over activated carbon for CO₂-free hydrogen production, Int. J. Hydrog. Energy 32 (2007) 4792–4799, <https://doi.org/10.1016/j.ijhydene.2007.07.041>.
- [14] W.H. Chen, H.J. Liou, C.I. Hung, A numerical approach of interaction of methane thermocatalytic decomposition and microwave irradiation, Int. J. Hydrog. Energy 38 (2013) 13260–13271, <https://doi.org/10.1016/j.ijhydene.2013.07.107>.
- [15] S. Gadkari, B. Fidalgo, S. Gu, Numerical analysis of microwave assisted thermocatalytic decomposition of methane, Int. J. Hydrog. Energy 42 (2017) 4061–4068, <https://doi.org/10.1016/j.ijhydene.2016.09.126>.

[16] B. Fidalgo, Y. Fernández, A. Domínguez, J.J. Pis, J.A. Menéndez, Microwave-assisted pyrolysis of CH₄/N₂ mixtures over activated carbon, *J. Anal. Appl. Pyrolysis* 82 (2008) 158–162, <https://doi.org/10.1016/j.jaap.2008.03.004>.

[17] M. Dadsetan, M.F. Khan, M. Salakhi, E.R. Bobicki, M.J. Thomson, CO₂-free hydrogen production via microwave-driven methane pyrolysis, *Int. J. Hydrom. Energy* 48 (2023) 14565–14576, <https://doi.org/10.1016/j.ijhydene.2022.12.353>.

[18] D. Fu, X. Zeng, J. Zou, H. Qian, X. Li, X. Xiong, Direct synthesis of Y-junction carbon nanotubes by microwave-assisted pyrolysis of methane, *Mater. Chem. Phys.* 118 (2009) 501–505, <https://doi.org/10.1016/j.matchemphys.2009.08.032>.

[19] A.V. Chistyakov, G.I. Konstantinov, M.V. Tsodikov, A.L. Maximov, Rapid conversion of methane to hydrogen stimulated by microwave irradiation on the surface of a carbon adsorbent, *Dokl. Phys. Chem.* 498 (2021) 49–53, <https://doi.org/10.1134/S0012501621050018>.

[20] M. Vázquez, E. Prato, Carbon nanotubes and microwaves, *ACS Nano* 3 (2009) 3819–3824.

[21] W. Lin, K. Moon, S. Zhang, Y. Ding, J. Shang, M. Chen, C. Wong, Less Defective, XXX (2010).

[22] C. Jiang, I.W. Wang, X. Bai, S. Balyan, B. Robinson, J. Hu, W. Li, A. Deibel, X. Liu, F. Li, L.M. Neal, J. Dou, Y. Jiang, R. Dagle, J.A. Lopez-Ruiz, G. Skoptsov, Methane catalytic pyrolysis by microwave and thermal heating over carbon nanotube-supported catalysts: productivity, kinetics, and energy Efficiency, *Ind. Eng. Chem. Res.* 61 (2022) 5080–5092, <https://doi.org/10.1021/acs.iecr.1c05082>.

[23] T. Christiansen, B. Robinson, A. Caiola, C. Jiang, J. Hu, Improved efficiency of the microwave-enhanced catalytic pyrolysis of methane through supplemental thermal heating, *Ind. Eng. Chem. Res.* (2022).

[24] B. Malecka, A. Lacz, E. Drozdz, A. Malecki, Thermal decomposition of d-metal nitrates supported on alumina, *J. Therm. Anal. Calorim.* 119 (2015) 1053–1061, <https://doi.org/10.1007/s10973-014-4262-9>.

[25] A. Baylet, P. Marecöt, D. Duprez, P. Castellazzi, G. Groppi, P. Forzatti, In situ Raman and in situ XRD analysis of PdO reduction and Pd⁰ oxidation supported on γ-Al₂O₃ catalyst under different atmospheres, *Phys. Chem. Chem. Phys.* 13 (2011) 4607–4613, <https://doi.org/10.1039/c0cp01331e>.

[26] J.Y. Kim, J.A. Rodriguez, J.C. Hanson, A.I. Frenkel, P.L. Lee, Reduction of CuO and Cu₂O with H₂: H embedding and kinetic effects in the formation of suboxides, *J. Am. Chem. Soc.* 125 (2003) 10684–10692, <https://doi.org/10.1021/ja0301673>.

[27] I. Pedroarena, L. Grande, J.J. Torrez-Herrera, S.A. Korili, A. Gil, Analysis by temperature-programmed reduction of the catalytic system Ni-Mo-Pd/Al₂O₃, *Fuel* 334 (2023), 126789, <https://doi.org/10.1016/j.fuel.2022.126789>.

[28] C. Jayaseelan, A.A. Rahuman, R. Ramkumar, P. Perumal, G. Rajakumar, A. V. Kirthi, T. Santhoshkumar, S. Marimuthu, Effect of sub-acute exposure to nickel nanoparticles on oxidative stress and histopathological changes in Mozambique tilapia, *Oreochromis mossambicus*, *Ecoxicol. Environ. Saf.* 107 (2014) 220–228.

[29] Y. Sahoo, Y. He, M.T. Swihart, S. Wang, H. Luo, E.P. Furlani, P.N. Prasad, An aerosol-mediated magnetic colloid: study of nickel nanoparticles, *J. Appl. Phys.* 98 (2005), <https://doi.org/10.1063/1.2033145>.

[30] M. Raja, J. Shuba, F.B. Ali, S.H. Ryu, Synthesis of copper nanoparticles by electroreduction process, *Mater. Manuf. Process.* 23 (2008) 782–785, <https://doi.org/10.1080/10426910802382080>.

[31] B.S. Kwak, B.H. Choi, M.J. Ji, S.M. Park, M. Kang, Synthesis of spherical NiO nanoparticles using a solvothermal treatment with acetone solvent, *J. Ind. Eng. Chem.* 18 (2012) 11–15, <https://doi.org/10.1016/j.jiec.2011.11.047>.

[32] T.P. Beebe, D.W. Goodman, B.D. Kay, J.T. Yates, Kinetics of the activated dissociative adsorption of methane on the low index planes of nickel single crystal surfaces, *J. Chem. Phys.* 87 (1987) 2305–2315, <https://doi.org/10.1063/1.453162>.

[33] Y. Shen, A.C. Lua, Synthesis of Ni and Ni-Cu supported on carbon nanotubes for hydrogen and carbon production by catalytic decomposition of methane, *Appl. Catal. B Environ.* 164 (2015) 61–69, <https://doi.org/10.1016/j.apcatb.2014.08.038>.

[34] B. Ali, S.M. Tasirin, P. Aminayi, Z. Yaakob, N.T. Ali, W. Noori, Non-supported nickel-based coral sponge-like porous magnetic alloys for catalytic production of syngas and carbon bio-nanofilaments via a biogas decomposition approach, *Nanomaterials* 8 (2018) 1–28, <https://doi.org/10.3390/NANO8121053>.

[35] A. Martínez de Yusó, J.M. Le Meins, Y. Oumellal, V. Paul-Boncour, C. Zlatea, C. Matei Ghimeş, Facile and rapid one-pot microwave-assisted synthesis of Pd-Ni magnetic nanoalloys confined in mesoporous carbons, *J. Nanopart. Res.* 18 (2016), <https://doi.org/10.1007/s11051-016-3682-9>.

[36] K.Y. Park, J.H. Han, S.B. Lee, J.W. Yi, Microwave absorbing hybrid composites containing Ni-Fe coated carbon nanofibers prepared by electroless plating, *Compos. Part A Appl. Sci. Manuf.* 42 (2011) 573–578, <https://doi.org/10.1016/j.compositesa.2011.01.020>.

[37] Y. Liu, C. Qiang, Magnetic properties and microwave absorption properties of short carbon fibres coated by Ni-Fe alloy coatings, *Bull. Mater. Sci.* 38 (2015) 1673–1678, <https://doi.org/10.1007/s12034-015-1106-6>.

[38] S.T. Kim, S.S. Kim, Microwave absorbance of Ni-Fe thin films on hollow ceramic microspheres dispersed in a rubber matrix, *J. Alloy. Compd.* 687 (2016) 22–27, <https://doi.org/10.1016/j.jallcom.2016.06.042>.

[39] E.R. Beach, K. Shqau, S.E. Brown, S.J. Rozeveld, P.A. Morris, Solvothermal synthesis of crystalline nickel oxide nanoparticles, *Mater. Chem. Phys.* 115 (2009) 371–377, <https://doi.org/10.1016/j.matchemphys.2008.12.018>.